Mechanical Stability of Polystyrene and Janus Particle Monolayers at the Air/Water Interface

Jessica Lenis,[†,‡,‖] Sepideh Razavi,[†,⊥,‖] Kathleen D. Cao,[‡] Binhua Lin,[§] Ka Yee C. Lee,[‡] Raymond S. Tu,[†] and Ilona Kretzschmar*[,†]

[†]Department of Chemical Engineering, City College of City University of New York, New York, New York 10031, United States

[‡]Department of Chemistry, Institute for Biophysical Dynamics, and James Franck Institute, The University of Chicago, Chicago, Illinois 60637, United States

[§]James Franck Institute and Center for Advanced Radiation Sources, The University of Chicago, Chicago, Illinois 60637, United States

ⓢ *Supporting Information*

ABSTRACT: The compressional instability of particle-laden air/water interfaces is investigated with plain and surface-anisotropic (Janus) particles. We hypothesize that the amphiphilic nature of Janus particles leads to both anisotropic particle–particle and particle–interface interactions that can yield particle films with unique collapse mechanisms. Analysis of Langmuir isotherms and microstructural characterization of the homogeneous polystyrene particle films during compression reveal an interfacial buckling instability followed by folding, which is in good agreement with predictions from classical elasticity theory. In contrast, Janus particle films exhibit a different behavior during compression, where the collapse mode occurs through the subduction of the Janus particle film. Our results suggest that particle-laden films comprised of surface-anisotropic particles can be engineered to evolve new material properties.

The behavior of particles at fluid/fluid interfaces has captured the interest of many researchers.[1−4] Numerous uses have been suggested, ranging from the control of non-equilibrium droplet shapes[5−7] to the creation of "Pickering" emulsions for drug delivery.[8,9] More recently, the application of anisotropic particles, in terms of either shape (e.g., ellipsoidal, cylindrical, dumbbell- and disk-shaped, and cubic)[10−12] or chemistry (e.g., Janus and patchy),[13−18] has been suggested as a method to tune interparticle interactions, controlling both interfacial microstructure and assembly behavior, as well as defining the interfacial mechanics.[19−22] These anisotropic systems are particularly interesting because the nature of the anisotropy can be precisely engineered to control instabilities at a fluid/fluid interface.

The behavior of homogeneous particles partitioning into a fluid/fluid interface has been well-studied, where the elastic modulus is governed by particle–particle interactions such as electrostatic and capillary interactions.[23−25] These types of systems can result in stiff interfacial particle films that buckle out-of-plane, yielding an elastic modulus of $E \approx 100$ mN/m,[26] where the modulus is sensitive to the capping ligands on the particle surface. Moreover, using anisotropic amphiphilic particles at the interface has been suggested as a method to control the

adsorption energy to a fluid/fluid interface[27] and the interparticle interactions in the plane of the interface.[17] Recent work has shown that these systems can behave as analogues to surfactants, defining both the stability and shape of the fluid/fluid interface by tuning the particle anisotropy.[28]

In this work, we describe the collapse mechanism of Janus particle (JP) films under compressive stress and contrast the behavior to isotropic particle films that buckle at the air/water interface. We use a Langmuir trough to characterize the isothermal compression and expansion of the particle laden air/water interface. Simultaneously, we visualize the changes in the microstructure of homogeneous polystyrene (PS) particle and anisotropic, gold-capped JP films. Using plain PS particles, we observe the expected surface instabilities associated with buckling under compression, but using Janus particles, we observe a different collapse mechanism, namely subduction. These results suggest that anisotropic particles can be applied to control mechanical properties of interfacial particle layers to engineer tunable materials.

Sulfated PS particles, 2.4 ± 0.1 μm in diameter, from Invitrogen are used for all experiments. Gold-capped Janus particles are prepared by depositing the PS particles as a monolayer on pre-cleaned microscope slides followed by metal evaporation. The deposition of metal occurs in two steps, (1) a 5 nm titanium adhesive layer and (2) a 20 nm gold cap, as described previously.[29] Subsequently, the anisotropic particles are sonicated off the glass slides into water contained in a Petri dish. The Petri dish with the particle suspension is then dried in an oven at ∼70 °C until all water has evaporated. The dried particles are transferred into a glass vial and weighed, typically yielding JP powder of 30 ± 5 mg. All glassware is thoroughly cleaned using a sulfuric acid (Certified ACS Plus, Fisher Scientific) and NOCHROMIX (Godax Laboratories, Inc.) mixture, followed by rinsing with copious amounts of ultrapure water and vacuum drying. Water used throughout the study has a resistivity of 18.2 MΩ·cm and is obtained from an Advantage A10 Milli-Q System (EMD Millipore, Billerica, MA). An aqueous mixture of 1.985 M NaCl and 0.4 M glucose is used as a density-matched subphase ($\rho_{sub} = 1.088$ g/cm^3) to ensure efficient

trapping at the interface (ρ_{PS} = 1.055 g/cm^3 and ρ_{JP} ≈ 1.283 g/cm^3). Owing to the repulsive particle–interface interaction, which arises from the negative charge on the particle surface and the negatively charged air/water interface,[30] addition of salt is required to obtain appreciable particle trapping at the interface. Consequently, the salt in the subphase screens the electrostatic repulsion between individual PS particles, increasing the propensity to cluster.

A PTFE Langmuir trough (NIMA, UK) with two barriers and an initial surface area of 78 cm^2 is used to form the particle film at the air/water interface and to carry out isothermal compression and expansion measurements at 0.12 ± 0.08 cm^2/s. The trough is housed on the stage of an Olympus bright field microscope with a 10× objective sitting atop a vibration isolation table, and images of the surface morphology of the particle film are recorded with a charge-coupled-device camera. A paper Wilhelmy plate oriented parallel to the barriers is used to measure the surface pressure, π, i.e., the difference in surface tension between a pure air/water interface and one laden with particles. All experiments are performed at room temperature (21−23 °C).

The particle film on the Langmuir trough is prepared by spreading a 1:3 aqueous particle:isopropyl alcohol mixture onto the air/water interface. A particle concentration of 10 mg/mL is used for both systems. It is necessary to sonicate the particle solution for 5 min before spreading to reduce particle aggregation. The system is allowed to equilibrate for about 15 min before the initial compression to ensure adequate evaporation of the solvent.

Upon deposition onto the liquid subphase, some level of clustering or aggregation of the plain PS particles is immediately observed. Initial compression and subsequent expansion of the film give rise to t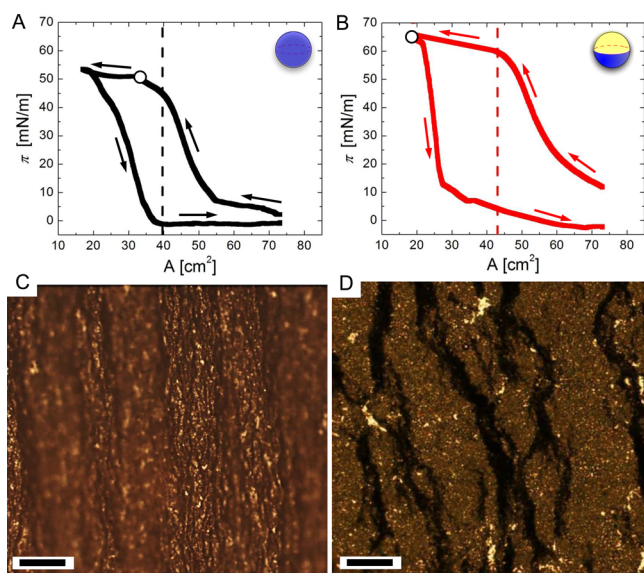he isotherm shown in Figure 1A. As the film is compressed, microscopic observations (see Supporting Information, Figure S1A and Video S1) reveal that the particles are pushed to pack more tightly together and eventually attain a close-packed structure with an area fraction of ϕ = 0.78 ± 0.03 obtained from analyzing image frames just before out-of-plane deformations are observed. Compression beyond this configuration gives rise to striation patterns in the film pointing to the onset of out-of-plane deformations. These observations are in accordance with findings from our recent study on 1 μm silica particle monolayers at the air/water interface.[31] When the film is further compressed into the plateau region of the isotherm (∼45 mN/m), compression of the film no longer elicits a large increase in surface pressure, suggesting that the film is relieving the lateral stress by collapse via out-of-plane deformation (dashed line). Indeed, wrinkles on the particle film can be identified at surface pressures of π ≥ 45 mN/m, and their formation brings parts of the film out of the focal plane. The wrinkles become more pronounced as the compression proceeds, with a pattern of wrinkles becoming clearly discernible at a surface pressure, π, of ∼49 mN/m (see Figure 1C). Analysis of several images in this region gives rise to an average wrinkling wavelength, λ, of 289 ± 81 μm, with the wrinkle direction closely aligned with the barriers. As the particle film is compressed more, the monolayer further relieves the lateral stress by forming folds. These folded structures are found to be reversible and materials in the folded regions are reintroduced to the 2D interface upon expansion. Upon further expansion, the film ruptures into clusters of tightly packed particles resulting in the observed hysteresis in the isotherm.

When Janus particles are spread onto the liquid subphase, the particles form dendritic clusters similar to observations reported by Lee et al.[28] for Janus particles at the decane/water interface. While aggregation of particles is clearly observed within a cluster, cluster−cluster interactions are not apparent. Figure 1B shows the isotherm of the first compression−expansion cycle for the JP film, which exhibits similar features to the isotherm obtained for the PS particle layer (Figure 1A), though the JP film is capable of attaining a higher surface pressure. However, microscopic observations reveal significant differences (see Supporting Information, Figure S1B and Video S2). Upon compression, the JP clusters move toward one another but do not merge. This behavior gives rise to voids (light areas) in the interface where JP-free regions exist at the early stages of compression. As the JP film is compressed to the trough area indicated by the dashed line shown in Figure 1B, dark patches start to emerge. Close examination of the microscope images at 50× magnification suggests that these dark patches are likely resulting from the sliding of one layer of particles under another, creating a subduction zone (black patch) in the process (Supporting Information, Video S3). Compression beyond the turning point does not yield any wrinkles, but instead subduction zones can be found throughout the layer (see Figure 1D, π ≈ 66 mN/m). Upon expansion the subduction zones stay intact and the particle film ruptures along the edges of the subduction zones resulting in the observed hysteresis in the isotherm.

In order to verify the subduction mechanism in the JP case, the growth rate of the black patches is compared to the compression rate of the trough barriers in the range of π ≈ 63 (t = 360 s) to π ≈ 65 mN/m (t = 440 s). Analysis of the subduction zone growth (Figure 2) yields a rate of 0.129 cm^2/s after correction for void reduction during compression, which correlates with the rate of area loss rendered by the compression process within the same time frame (0.127 cm^2/s), supporting the different mode of

Figure 1. Compression−expansion isotherms of 2.4 μm (A) plain and (B) gold-coated Janus polystyrene particle layer at an air/water interface. The two films show different collapse behaviors: optical microscopy image of (C) the plain polystyrene particle layer at a surface pressure of 49 mN/m shows buckling instability, whereas that of (D) the Janus particle layer at a surface pressure of 66 mN/m shows subduction instability. The dashed lines in the isotherms indicate the onset of layer instability in the two particle films during compression; the circle on each isotherm identifies the pressure at which the corresponding image is taken. Scale bars are 100 μm.
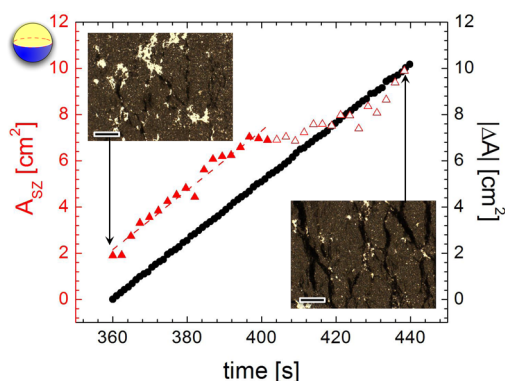
Figure 2. Total area of subduction zones (A_{SZ}, red triangles, left axis) corrected for void reduction, and total trough area decrease ($|\Delta A|$, solid black circles, right axis) as a function of time upon compression of a Janus polystyrene particle film at the air/liquid interface from $\pi \approx 63$ ($t = 360$ s) to $\pi \approx 65$ mN/m ($t = 440$ s). Solid red triangles indicate portion of subduction zone data fitted to determine rate of subduction (0.129 cm^2/s). Insets show optical micrographs of the film at the respective time stamps. Scale bars are 200 μm.

instability for the JP film. At a later stage of compression (400–420 s), black patch formation stagnates, indicating black patch formation outside the field of view, but then picks up again beyond 420 s when the formation of black patches resumes within the area of analysis. In the JP films, the concurrence of the rate of subduction zone formation and the rate of compression implies the formation of bilayer structures throughout the interfacial particle film. Moreover, owing to layer stacking in the black patches formed, the final pressure that the JP film can withstand in a closed-barrier state is 30% higher than that of the pure PS film, also in line with the proposed subduction mechanism. Analogous experiments carried out using smaller polystyrene (0.960 ± 0.016 μm) and gold-capped Janus polystyrene particles reveal similar isotherms and microstructures indicating that the subduction behavior is a general phenomenon for gold-capped Janus polystyrene particles (see Supporting Information, Figure S2).

Our results show that we can tune film stability to evolve a new mode of monolayer collapse at higher compressional stresses by controlling the surface properties of the particles. The collapse mechanisms for (A) a plain and (B) a gold-capped Janus polystyrene particle film are illustrated in Figure 3. The PS particle layer is formed because of isotropic capillary interactions between individual PS particles that give rise to a cohesive layer capable of withstanding large compressions. The resulting elastic sheet undergoes wrinkling with a wrinkling wavelength, λ,
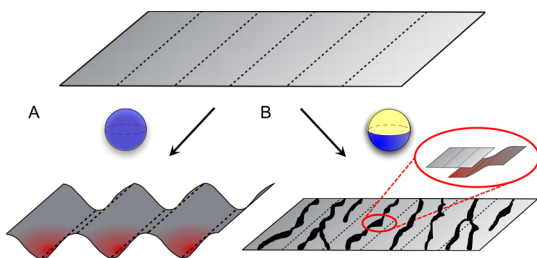

Figure 3. Schematic depiction of collapse mechanisms for (A) a plain and (B) a Janus polystyrene particle film at an air/water interface. The plain particle film undergoes a wrinkling transition, whereas the Janus particle film collapses via a subduction mechanism.

measured to be 289 ± 81 μm, in reasonable agreement with $\lambda = 350 \pm 12$ μm predicted using classical elasticity theory with an area packing fraction of $\varphi = 0.78 \pm 0.03$ and a Poisson ratio of $\nu = 1/\sqrt{3}$.[25] In contrast, the JP film, while exhibiting a similar isotherm behavior, collapses via a subduction mechanism that likely originates from the impact of particle orientation that influences the film's structure (i.e., presence of voids and black patches) which in turn affects the mechanical properties of the JP monolayer.

Figure 4A displays an SEM image of the JP layer formed under compression at the interface and deposited on a silicon wafer
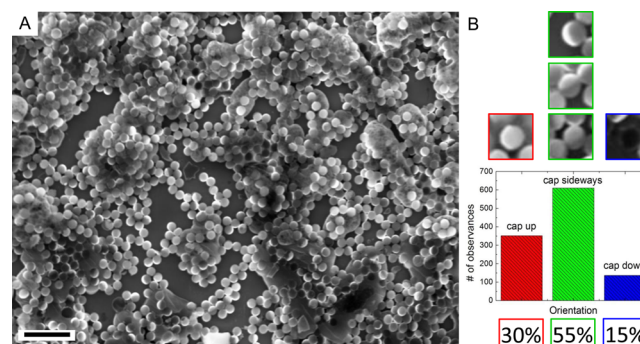

Figure 4. (A) Scanning electron micrograph of a 2.4 μm Janus particle layer deposited on a silicon wafer via the inverse Langmuir–Schaefer transfer method at a compressed state. The scale bar is 10 μm. (B) Histogram of orientations of 1100 particles separated into cap-up, cap-sideways, and cap-down orientations.

using the inverse Langmuir–Schaefer transfer method at the closed-barrier state (see Supporting Information, Figure S3).[32,33] It has been demonstrated that the transferred film's fidelity to the free-standing film is preserved for transfers made at such a compressed state. The bright side of each particle represents the gold cap (high electron density), whereas the darker regions indicate the PS base particles (low electron density). During drying of the subphase, glucose and NaCl precipitate leading to a glucose residue (non-spherical material in the SEM image) and large NaCl cubic crystals (not shown). By investigating the orientation of more than 1000 particles, the frequency of different cap orientations such as cap-up, cap-sideways, and cap-down is approximated to be 30%, 55%, and 15%, respectively, as shown in the histogram (Figure 4B). In addition, the JP layers in Figure 4A are found to be non-planar, while the PS particle layers show planar particle clusters with close packing (Supporting Information, Figure S4). From the analysis, it can be inferred that Janus polystyrene particles with unmodified gold caps are randomly oriented at the air/water interface with the majority of the particles exhibiting a sideways configuration (55%). This finding of randomness in JP orientation is in line with earlier observations by Lee et al.,[28] who reported a distribution of 55% (up), 30% (sideways), and 15% (down) for gold-capped Janus polystyrene particles at the decane/water interface. The random orientation of the particles at the interface is a result of the limited amphiphilicity obtained when gold and PS are paired as the two faces of a Janus particle; i.e., the Janus balance is very low ($\Theta_{Au} = (43 \pm 2)°$ and $\Theta_{PS} < 30°$),[34,35] which is not sufficient to orient the Janus particles in an upright configuration.

The random orientation of the Janus particles at the air/water interface leads to non-uniform capillary interactions between particles, owing to the fact that the particle–particle interactions strongly depend on the specific particle sides that face one

another in each interacting particle pair; i.e., the type and strength of these interactions vary at different locations throughout the JP monolayer impacting its cohesiveness. We speculate that the random orientation of Janus particles at the interface gives rise to local anisotropic zones that promote an anisotropic stress distribution. This anisotropy leads to passive percolation defects at which subduction occurs. Experiments currently underway focus on modification of the gold cap to tune particle orientation at the interface and explore its impact on the compressional behavior of the JP layers to further support our mechanistic proposal. In addition, one can envision that mixtures of polystyrene and Janus particles at the interface may enable formation of particle films with regions that subduct and wrinkle in well-defined areas thereby creating particle films with tunable optical properties. Another interesting approach to pre-aligned Janus particles could be Nie et al.'s[36] recently introduced electrospray deposition at the air/water interface that could potentially enable the formation of bilayer mimics.

ASSOCIATED CONTENT

Ⓢ Supporting Information

The Supporting Information is available free of charge on the ACS Publications website at DOI: 10.1021/jacs.5b10183.

> Optical micrographs, pressure isotherms, and microscopy images of plain polystyrene and gold-coated Janus polystyrene particle layers; details of the inverse Langmuir–Schaefer transfer technique; scanning electron micrograph of a 2.4 μm PS particle layer in the compressed state (PDF)
>
> Video S1, polystyrene particles at the air/water interface under compression (AVI)
>
> Video S2, Janus particles at the air/water interface under compression (AVI)
>
> Video S3, subduction for a JP monolayer during compression (AVI)

AUTHOR INFORMATION

Corresponding Author
*kretzschmar@ccny.cuny.edu

Present Address
⊥S.R.: Department of Chemical Engineering, University of Michigan, Ann Arbor, MI 48109, USA.

Author Contributions
∥J.L. and S.R. contributed equally.

Notes
The authors declare no competing financial interest.

ACKNOWLEDGMENTS

REFERENCES

(1) Dinsmore, A. D.; Hsu, M. F.; Nikolaides, M. G.; Marquez, M.; Bausch, A. R.; Weitz, D. A. *Science* **2002**, *298*, 1006.
(2) Manoharan, V. N. *Science* **2015**, *349*, 6251.
(3) Manoharan, V. N. *Nat. Mater.* **2015**, *14*, 869.
(4) Boniello, G.; Blanc, C.; Fedorenko, D.; Medfai, M.; Mbarek, N. B.; In, M.; Gross, M.; Stocco, A.; Nobili, M. *Nat. Mater.* **2015**, *14*, 908.
(5) Pawar, A. B.; Caggioni, M.; Ergun, R.; Hartel, R. W.; Spicer, P. T. *Soft Matter* **2011**, *7*, 7710.
(6) Cui, M.; Emrick, T.; Russell, T. P. *Science* **2013**, *342*, 460.
(7) Wu, T.; Wang, H.; Jing, B.; Liu, F.; Burns, P. C.; Na, C. *Nat. Commun.* **2015**, *6*, 5929.
(8) Tan, A.; Simovic, S.; Davey, A. K.; Rades, T.; Prestidge, C. A. *J. Controlled Release* **2009**, *134*, 62.
(9) Zarzar, L. D.; Sresht, V.; Sletten, E. M.; Kalow, J. A.; Blankschtein, D.; Swager, T. M. *Nature* **2015**, *518*, 520.
(10) Madivala, B.; Fransaer, J.; Vermant, J. *Langmuir* **2009**, *25*, 2718.
(11) de Folter, J. W. J.; Hutter, E. M.; Castillo, S. I. R.; Klop, K. E.; Philipse, A. P.; Kegel, W. K. *Langmuir* **2014**, *30*, 955.
(12) Morgan, A. R.; Ballard, N.; Rochford, L. A.; Nurumbetov, G.; Skelhon, T. S.; Bon, S. A. F. *Soft Matter* **2013**, *9*, 487.
(13) DeGennes, P. G. *Angew. Chem., Int. Ed. Engl.* **1992**, *31*, 842.
(14) Walther, A.; Müller, A. H. E. *Chem. Rev.* **2013**, *113*, 5194.
(15) Ruhland, T. M.; Gröschel, A. H.; Ballard, N.; Skelhon, T. S.; Walther, A.; Müller, A. H. E.; Bon, S. A. F. *Langmuir* **2013**, *29*, 1388.
(16) Tu, F.; Lee, D. *Chem. Commun.* **2014**, *50*, 15549.
(17) Fernandez-Rodriguez, M. A.; Rodriguez-Valverde, M. A.; Cabrerizo-Vilchez, M. A.; Hidalgo-Alvarez, R. *Adv. Colloid Interface Sci.* **2015**, DOI: 10.1016/j.cis.2015.06.002.
(18) Bahrami, R.; Löbling, T. I.; Gröschel, A. H.; Schmalz, H.; Müller, A. H. E.; Altstädt, V. *ACS Nano* **2014**, *8*, 10048.
(19) Adams, D. J.; Adams, S.; Melrose, J.; Weaver, A. C. *Colloids Surf., A* **2008**, *317*, 360.
(20) Ballard, N.; Bon, S. A. F. J. *J. Colloid Interface Sci.* **2015**, *448*, 533.
(21) Tu, F.; Lee, D. J. *J. Am. Chem. Soc.* **2014**, *136*, 9999.
(22) Tu, F.; Park, B. J.; Lee, D. *Langmuir* **2013**, *29*, 12679.
(23) Monteux, C.; Kirkwood, J.; Xu, H.; Jung, E.; Fuller, G. G. *Phys. Chem. Chem. Phys.* **2007**, *9*, 6344.
(24) Leahy, B. D.; Pocivavsek, L.; Meron, M.; Lam, K. L.; Salas, D.; Viccaro, P. J.; Lee, K. Y. C.; Lin, B. *Phys. Rev. Lett.* **2010**, *105*, 058301.
(25) Vella, D.; Aussillous, P.; Mahadevan, L. *Europhys. Lett.* **2004**, *68*, 212.
(26) You, S. S.; Rashkov, R.; Kanjanaboos, P.; Calderon, I.; Meron, M.; Jaeger, H. M.; Lin, B. *Langmuir* **2013**, *29*, 11751.
(27) Binks, B. P.; Fletcher, P. D. I. *Langmuir* **2001**, *17*, 4708.
(28) Park, B. J.; Brugarolas, T.; Lee, D. *Soft Matter* **2011**, *7*, 6413.
(29) Pawar, A. B.; Kretzschmar, I. *Langmuir* **2008**, *24*, 355.
(30) Beloqui Redondo, A.; Jordan, I.; Ziazadeh, I.; Kleibert, A.; Giorgi, J. B.; Wörner, H. J.; May, S.; Abbas, Z.; Brown, M. A. *J. Phys. Chem. C* **2015**, *119*, 2661.
(31) Razavi, S.; Cao, K. D.; Lin, B.; Lee, K. Y. C.; Tu, R. S.; Kretzschmar, I. *Langmuir* **2015**, *31*, 7764.
(32) Lee, K. Y. C.; Lipp, M. M.; Takamoto, D. Y.; Ter-Ovanesyan, E.; Zasadzinski, J. A.; Waring, A. J. *Langmuir* **1998**, *14*, 2567.
(33) Frey, S. L.; Chi, E. Y.; Arratia, C.; Majewski, J.; Kjaer, K.; Lee, K. Y. C. *Biophys. J.* **2008**, *94*, 3047.
(34) Shemi, O.; Solomon, M. J. *Langmuir* **2014**, *30*, 15408.
(35) Aveyard, R.; Clint, J. H.; Nees, D.; Paunov, V. N. *Langmuir* **2000**, *16*, 1969.
(36) Nie, H.-L.; Dou, X.; Tang, Z.; Jang, H. D.; Huang, J. *J. Am. Chem. Soc.* **2015**, *137*, 10683.